Computers in Industry 64 (2013) 1221–1228

Contents lists available at SciVerse ScienceDirect

Computers in Industry

journal homepage: www.elsevier.com/locate/compind

Direct regularized surface reconstruction from gradients for Industrial Photometric Stereo

Matthew Harker *, Paul O'Leary

University of Leoben, Peter-Tunner-Strasse 27, 8700 Leoben, Austria

ARTICLE INFO

Article history:
Received 26 September 2012
Received in revised form 22 March 2013
Accepted 27 March 2013
Available online 3 July 2013

Keywords:
Photometric Stereo
Gradient field
Tikhonov regularization
Numerical linear algebra

ABSTRACT

This paper addresses the issue of regularization in the surface reconstruction from gradients problem in Industrial Photometric Stereo. Regularization of the solution is a necessary step in an industrial environment, where algorithms must cope with non-Gaussian noise, such as outliers, or non-Lambertian textures such as corrosion. Introducing Tikhonov regularization into the global least squares solution suppresses the influence of outliers in the reconstruction. Viable methods should both minimize a global least squares cost function and also introduce some form of regularization into the solution; state-of-the-art methods to this end are grossly inefficient and are severely limited in the size of surface they can reconstruct. We present a new algorithm which can reconstruct a surface of 1200×1200, (i.e., greater than 1 M-pixel) in a few seconds. This is orders of magnitude faster than state-of-the-art methods incorporating regularization, and hence presents the first method viable for regularized reconstructions in practical applications.

© 2013 Published by Elsevier B.V.

1. Introduction

In the steel industry, a given plant will concurrently produce steel of different qualities, consisting of different alloys. It is therefore critical to track the individual workpieces as they traverse the plant. For this purpose the steel bars are stamped with a code, which must be robust with respect to high temperatures, scaling, etc., and must also be human readable. The present solution is to stamp human readable codes into the ends of the steel bars. Thus, automating the code reading process is a task of 3D surface measurement.

1.1. Regularization of surface reconstruction

Photometric Stereo [1] is a method for obtaining 3D depth information from a single view, and inasmuch is an attractive method for 3D measurements in industrial applications. The method uses different lighting conditions to essentially measure the gradient field of a surface. Thus, since the gradient field can be considered to be a measurement, it is necessarily corrupted by noise of one form or another. Consequently, any algorithm for reconstructing the surface from its gradient field must account for noise. For example, if the noise can be considered to be independent and identically distributed (i.i.d.) Gaussian noise, then the appropriate solution should minimize a global least squares cost function. Industrial environments, however, are usually not so forgiving as to provide Gaussian noise. Real lighting illuminating real surfaces can induce specular reflections resulting in saturated image pixels. Furthermore, real surfaces are generally not Lambertian in terms of scattering properties due, for example, to corrosion and other sources; hence, some of the basic assumptions of Photometric Stereo are compromised. Thus to cope with more general forms of noise, such as outliers, regularization must be incorporated into the least squares regularization. One potential method for accomplishing this would be either a more general model for surface reflectance [2] or individually modelling imaging errors [3]. The approach proposed in this paper is to work directly with the gradient data, and impose Tikhonov regularization on the solution. Tikhonov regularization [4] is a common form of regularizing the solution of inverse problems; hence, the method proposed here should have longer reaching applications than just the surface reconstruction from gradients problem. Unfortunately, when it comes to surface reconstruction algorithms, there is always a tradeoff between quality of the results, and the speed in which they are obtained. High quality results tend to come from computationally intensive algorithms. In this paper, we aim to close the gap of this disparity and show that high quality regularized reconstructions can be obtained with reasonable computation time. To capture as much detail as possible in the 3D measurement process, one must utilize the full resolution of the camera. For industrial cameras, this means that the reconstruction of the surface must work expediently for surfaces of the order of 1000×1000, that is, for mega-pixel sized images. The apparatus for

* Corresponding author. Tel.: +43 03842 402 5309; fax: +43 03842 402 5302.
E-mail address: matthew.harker@unileoben.ac.at (M. Harker).

0166-3615/$ – see front matter © 2013 Published by Elsevier B.V.
http://dx.doi.org/10.1016/j.compind.2013.03.013

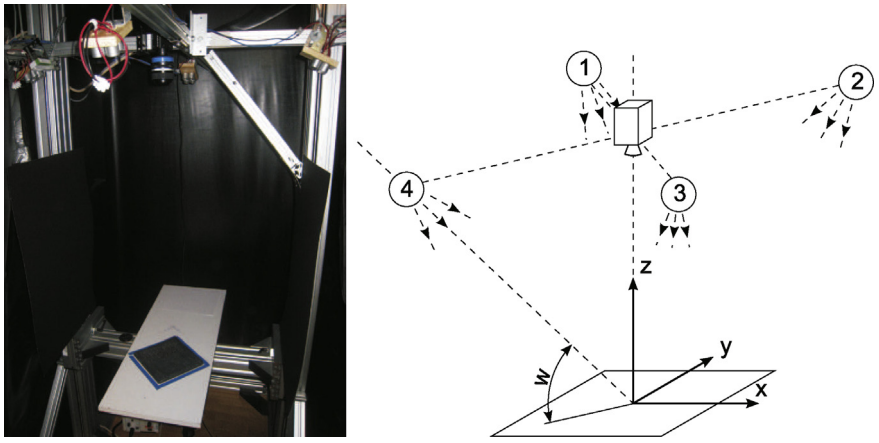

Fig. 1. The apparatus is a four light source Photometric Stereo rig.

testing the newly proposed algorithms is a four-source Photometric Stereo setup, shown in Fig. 1.

The task at hand is the 3D measurement of the ends of steel blocks, whereupon an identification code has been stamped; an example of such a surface is shown in Fig. 2.

1.2. Relevant literature

There is much literature on the reconstruction of a surface from its gradient field. They can be classified by their underlying assumptions: Path integral methods [5–8]: such methods use the principle that a path integral over a closed loop of an integrable gradient field should be zero. The difficulty with such methods is that they minimize local cost functions, and thus the error is unevenly distributed over the surface. Further, none of the methods implement any kind of regularization. Basis function methods [9–11]: these methods function by projecting the gradient field onto an integrable set of basis functions. Methods such as [9,10] use periodic basis functions, and hence cannot reconstruct surfaces as simple as $z = ax + by$, and thus have terrible least squares estimation properties. The method of Karaçalı [11] is unfortunately grossly inefficient and is limited to surfaces of size 32×32 due to memory requirements. Variational methods [9,12–16]: based on the calculus of variations, these methods minimize a functional subject to boundary conditions. The algorithms require the solution of Poisson's equation, for which there exist efficient numerical solutions [13]. Some types of boundary conditions, such as periodic boundary conditions yield efficient solutions [9], but can be largely unrealistic assumptions for industrial applications. Furthermore, when regularization is introduced, the efficient algorithms become unviable, and inefficient techniques such as vectorization are used, such as in [16]. Global least squares: in [17], a global least squares approach was taken, obtaining an efficient and numerically stable algorithm by means of relating the problem to a Sylvester equation – apparently for the first time. Regularized reconstruction [16,18–20]: methods such as [16,18,19] incorporate regularization into their solutions, but only by sacrificing efficiency. Their approach is to "vectorize" the solution surface, i.e., by writing,

$$Z = [\boldsymbol{z}_1 \quad \boldsymbol{z}_2 \quad \cdots \quad \boldsymbol{z}_n], \tag{1}$$

and vectorizing it as

$$\boldsymbol{z} = \mathrm{vec}(Z) = \begin{bmatrix} \boldsymbol{z}_1 \\ \vdots \\ \boldsymbol{z}_n \end{bmatrix}. \tag{2}$$

For an $m \times n$ surface, the resulting system of equations has a coefficient matrix of size $2mn \times mn$. The resulting algorithms are thus of order $\mathcal{O}(n^6)$, which is simply not viable for practical purposes. For example, in [18], a time of about 3.5 h to reconstruct a surface of size 240×314 was reported. Available code for the method in [19] is not functional on modern PC for a similar surface size. The image size alone is not adequate for a practical application. Hence state-of-the-art solutions for the large scale regularized reconstruction are non-existent. In [20] it was demonstrated that the regularized reconstruction problem could be cast in the same form as the global least squares solution [17], yielding for the first time an $\mathcal{O}(n^3)$ algorithm for regularized reconstruction. In this paper, by taking advantage of the structure of the problem, and invoking sparse matrix methods, we improve on the results of [17] by orders of magnitude (see Table 1). The new algorithm thus produces the first regularized reconstruction method which is viable in an industrial environment, with its associated time-constraints on the measurement. The form of regularization introduced, namely Tikhonov regularization, is a well established approach to regularizing the solution of inverse problems [4].

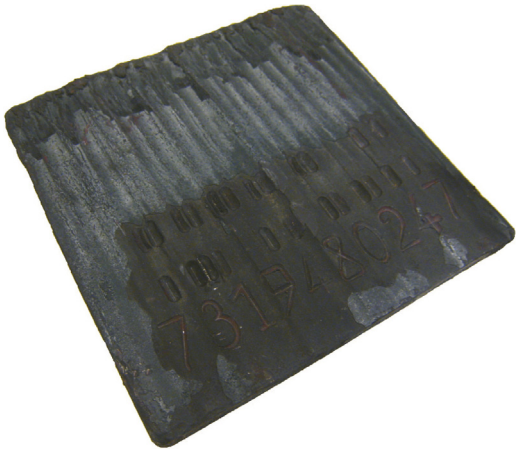

Fig. 2. An example of the surface to be measured. Note the various different textures due to scaling which make the Lambertian assumption questionable.

2. Mathematical background

2.1. Integration of a gradient field

The problem of surface reconstruction from a gradient field is equivalent to that of finding a potential function of a conservative

vector field. That is, given a gradient field,

$$\boldsymbol{G}(x,y) = \hat{z}_x(x,y)\boldsymbol{i} + \hat{z}_y(x,y)\boldsymbol{j}, \tag{3}$$

find a potential function $z(x,y)$ such that

$$\nabla z(x,y) = \boldsymbol{G}(x,y), \tag{4}$$

or equivalently,

$$\frac{\partial z(x,y)}{\partial x} = \hat{z}_x(x,y) \quad \text{and} \quad \frac{\partial z(x,y)}{\partial y} = \hat{z}_y(x,y). \tag{5}$$

By definition, if there exists such a potential function, $z(x,y)$, then the vector field is said to be conservative [21]. Recovering said potential function is thus an integration problem. To obtain the potential function, we integrate the x derivative with respect to x to yield,

$$z(x,y) = \int \hat{z}_x(x,y)\,\mathrm{d}x + C(y), \tag{6}$$

whereby the constant of integration can be a function of y. Since this potential function must yield the y derivative, we differentiate with respect to y and equate it to the gradient field's y-component, yielding,

$$\hat{z}_y(x,y) = \frac{\partial}{\partial y}\left(\int \hat{z}(x,y)dx\right) + C'(y). \tag{7}$$

Rearranging and integrating with respect to y yields the unknown function,

$$C(y) = \int \left(\hat{z}_y(x,y) - \frac{\partial}{\partial y}\left(\int \hat{z}_x(x,y)\,\mathrm{d}x\right)\right)\mathrm{d}y. \tag{8}$$

Note that since the surface is bivariate, the integral and differential in y of the second term do not "cancel". The recovered potential function is therefore,

$$z(x,y) = \int \hat{z}_x(x,y)\,\mathrm{d}x + \int \left(\hat{z}_y(x,y) - \frac{\partial}{\partial y}\left(\int \hat{z}_x(x,y)\,\mathrm{d}x\right)\right)\mathrm{d}y, \tag{9}$$

up to a constant of integration. Such an approach, however, assumes that the gradient field is integrable, that is, it satisfies the constraint

$$\frac{\partial}{\partial y}\hat{z}_x = \frac{\partial}{\partial x}\hat{z}_y. \tag{10}$$

Real measured gradient fields unfortunately contain noise, and generally do not satisfy this constraint. Various gradient field integration methods are based on approaches such as this [6,8]. However, these integration based methods do not account for noise in an uniform manner, as it accumulates as the numerical integration proceeds. Discrete versions of this algorithm can be very fast but they have two significant disadvantages: they have unfavourable least squares properties; and they do not incorporate any form of regularization. In Section 2.3, we take a global least squares approach to the reconstruction problem, and then subsequently derive a new algorithm which resolves these issues.

2.2. Numerical gradient integration

Working in the discrete domain, we can assume that the measured gradient field is a pair of $m \times n$ matrices (equivalently gray-scale images), $(\hat{Z}_x, \hat{Z}_y)$, i.e., in matrix notation. Integrating the x-derivative with respect to x, i.e., Eq. (6) in its discrete form, reads,

$$Z = \hat{Z}_x\Sigma_x^{\mathrm{T}} + \boldsymbol{g}\mathbf{1}^{\mathrm{T}}, \tag{11}$$

where Σ_x is a matrix effecting numerical indefinite integration (say, the coefficients of the trapezoidal rule), and $\boldsymbol{g}$ represents an unknown, discrete function in y. However, for the gradient to be consistent, we must have,

$$D_y Z = \hat{Z}_y, \tag{12}$$

where the matrix D_y effects numerical differentiation in the y-direction (see the following Section 2.3). Therefore, we must have that,

$$\hat{Z}_y = D_y\left(\hat{Z}_x\Sigma_x^{\mathrm{T}} + \boldsymbol{g}\mathbf{1}^{\mathrm{T}}\right) \tag{13}$$

Solving for the unknown $\boldsymbol{g}$ in the least squares sense yields,

$$\boldsymbol{g} = D_y^{+}\left(\hat{Z}_y - D_y\hat{Z}_x\Sigma_x^{\mathrm{T}}\right)(\mathbf{1}^{\mathrm{T}})^{+} \tag{14}$$

Finally, substituting this expression into the expression for Z in Eq. (11), yields the reconstructed surface. It can, however, be seen that this expression is largely asymmetric in x and y. We obtain a least squares estimation of $\boldsymbol{g}$, but not of Z which is desired. Alternatively, if we chose to first integrate in y and then find the unknown function in x, we would find a different expression. The expressions would only yield the same results when the gradient field is perfectly (numerically) integrable. This asymmetry is one of the downfalls of integration based methods.

2.3. Surface reconstruction as an inverse problem

To solve the surface reconstruction from gradients problem in the discrete domain, we propose to take a matrix based approach. From the theory of numerical differentiation [22], we have the well known central difference formula,

$$f'(x_0) = \frac{-f(x_0-h) + f(x_0+h)}{2h} \tag{15}$$

$$-\frac{h^2}{6}f^{(3)}(\xi_1) \quad \text{with} \quad \xi_1 \in [x_0-h, x_0+h]$$

which, when the error-term is truncated, yields a second order accurate derivative, when x_0 is the central point. If, however, x_0 is the first point in a sequence, we obtain the less-familiar end-point formula,

$$f'(x_0) = \frac{-3f(x_0) + 4f(x_0+h) - f(x_0+2h)}{2h} \tag{16}$$

$$+\frac{h^2}{3}f^{(3)}(\xi_0) \quad \text{with} \quad \xi_0 \in [x_0, x_0+2h].$$

which is also second order accurate when the error term is truncated. A similar formula for the last point in the sequence is obtained by substituting $h = -h$ into the last equation. We may then combine these equations into matrix form, thus obtaining a differential operator for any n point sequence (e.g., for a five point sequence),

$$\begin{bmatrix} f'(x_0) \\ f'(x_1) \\ f'(x_2) \\ f'(x_3) \\ f'(x_4) \end{bmatrix} \approx \frac{1}{2h}\begin{bmatrix} -3 & 4 & -1 & 0 & 0 \\ -1 & 0 & 1 & 0 & 0 \\ 0 & -1 & 0 & 1 & 0 \\ 0 & 0 & -1 & 0 & 1 \\ 0 & 0 & 1 & -4 & 3 \end{bmatrix}\begin{bmatrix} f(x_0) \\ f(x_1) \\ f(x_2) \\ f(x_3) \\ f(x_4) \end{bmatrix}. \tag{17}$$

Therefore, the operation of numerical differentiation can be effected by the matrix operation,

$$\boldsymbol{y}' = D\boldsymbol{y}. \tag{18}$$

It is also of note that formulas of a higher degree of accuracy can also be applied in this manner. For example, there are 5-point

formulas which are fourth order accurate given by,

$$D = \frac{1}{12h}\begin{bmatrix} -25 & 48 & -36 & 16 & -3 \\ -3 & -10 & 18 & -6 & 1 \\ 1 & -8 & 0 & 8 & -1 \\ -1 & 6 & -18 & 10 & 3 \\ 3 & -16 & 36 & -48 & 25 \end{bmatrix}, \tag{19}$$

which may, as with 3-point derivatives, be extended to a general n-point sequence. In this vein, the problem of the reconstruction of a surface from its gradient field can be formulated as finding a surface Z such that,

$$ZD_x^{\mathrm{T}} \approx \hat{Z}_x \qquad \text{and} \qquad D_y Z \approx \hat{Z}_y \tag{20}$$

where $(\hat{Z}_x, \hat{Z}_y)$ is the measured gradient field. Reconstruction in the least squares sense [17] can thus be formulated as the minimization of the functional,

$$\epsilon(Z) = \left\| ZD_x^{\mathrm{T}} - \hat{Z}_x \right\|_{\mathrm{F}}^2 + \left\| D_y Z - \hat{Z}_y \right\|_{\mathrm{F}}^2, \tag{21}$$

where the subscript 'F' denotes the Frobenius norm. The minimizing surface Z is the global least squares solution to the reconstruction problem. This solution is optimal when the errors in the measured gradient follow i.i.d. Gaussian distributions; in practice however, this is generally not the case. In Photometric Stereo, systematic errors are introduced, for example, by assuming a surface is Lambertian, which does not hold in many industrial applications. Furthermore, if noise in the image is Gaussian, noise in the gradient field will not be. Thus, to handle more general forms of noise, such as outliers, it is necessary to introduce Tikhonov regularization into the solution. For the surface reconstruction problem, this involves minimizing the functional,

$$\epsilon(Z) = \left\| ZD_x^{\mathrm{T}} - \hat{Z}_x \right\|_{\mathrm{F}}^2 + \left\| D_y Z - \hat{Z}_y \right\|_{\mathrm{F}}^2 + 2\lambda^2 \|Z - Z_0\|_{\mathrm{F}}^2, \tag{22}$$

where Z_0 is an a priori estimate of the reconstructed surface [20]. This can be extremely useful in industrial applications, where the a priori estimate can be the object's ideal designed geometry. If none is available, it can be assumed to be zero. The regularization term acts as a penalty term, which penalizes any deviation from the a priori estimate Z_0. The amount of regularization depends on the value of λ, which is a weighting ratio which favours either the least squares residual term, or the regularization term. Analysis of methods for determining λ, such as the L-curve method [23], is beyond the scope of this paper (see, e.g., [4]). The minimum of the functional is obtained by differentiating with respect to the unknown surface Z, obtaining,

$$(D_y^{\mathrm{T}} D_y + \lambda^2 I)Z + Z(D_x^{\mathrm{T}} D_x + \lambda^2 I) - D_y^{\mathrm{T}} \hat{Z}_y - \hat{Z}_x D_x - 2\lambda^2 Z_0 = 0 \tag{23}$$

This is a matrix equation, which is known as a Sylvester equation, and has the general form,

$$AZ + ZB + C = 0. \tag{24}$$

Expedient solutions exist, i.e., order $\mathcal{O}(n^3)$, however for larger surfaces this can become a tangible amount of computation, which may be prohibitive for industrial applications.

3. New approach

In the following, we take a new approach to solving the necessary equations for surface reconstruction from gradients, i.e., Eq. (23), by taking advantage of the following properties:

1. The structure and sparsity of the matrices in the problem.
2. The fact that significant computation can be performed offline.
3. Online computation can be performed in parallel. New versions of MATLAB® support parallel multi-core processing.

3.1. Algorithm description

In order to solve Eq. (23) efficiently, we first make the following definitions,

$$A = D_y^{\mathrm{T}} D_y \tag{25}$$

$$F(\lambda) = D_y^{\mathrm{T}} \hat{Z}_y + \hat{Z}_x D_x + 2\lambda^2 Z_0 \tag{26}$$

Secondly, we compute the eigen-decomposition[1] of the matrix $D_x^{\mathrm{T}} D_x$ such that,

$$D_x^{\mathrm{T}} D_x = USU^{\mathrm{T}}. \tag{27}$$

Since $D_x^{\mathrm{T}} D_x$ is symmetric semi-definite, the matrix U is orthogonal and the matrix S is diagonal with real positive eigenvalues (with a single zero eigenvalue), i.e.,

$$S = \mathrm{diag}\{0, s_2, s_3, \ldots, s_n\}. \tag{28}$$

With these definitions, Eq. (23) can now be written as,

$$(A + \lambda^2 I)Z + Z(USU^{\mathrm{T}} + \lambda^2 I) - F(\lambda) = 0 \tag{29}$$

By post-multiplying this equation by the matrix U, we obtain,

$$(A + \lambda^2 I)ZU + Z(US + \lambda^2 U) - F(\lambda)U = 0, \tag{30}$$

due to the orthogonality of U such that $U^{\mathrm{T}}U = I$. Factoring the second term yields the equation,

$$(A + \lambda^2 I)ZU + ZU(S + \lambda^2 I) - F(\lambda)U = 0, \tag{31}$$

For simplification, we can now make the substitutions

$$W = ZU \tag{32}$$

$$G(\lambda) = F(\lambda)U, \tag{33}$$

to yield,

$$(A + \lambda^2 I)W + W(S + \lambda^2 I) - G(\lambda) = 0, \tag{34}$$

The preceding reduction has been made to diagonalize the coefficient matrix of the second term; that is, the matrix $(S + \lambda^2 I)$ is diagonal, and post-multiplies into W. This essentially separates the matrix equation into a set of vector-valued equations; i.e., writing the equation column-wise, we have,

$$(A + \lambda^2 I)\boldsymbol{w}_k + (s_k + \lambda^2)\boldsymbol{w}_k - \boldsymbol{g}_k(\lambda) = \boldsymbol{0}, \quad \text{for} \quad k = 1, \ldots, n, \tag{35}$$

where $\boldsymbol{w}_k$ is the kth column of W, and similarly for $\boldsymbol{g}_k$. Thus, we may solve for the unknown W by solving the set of linear equations which simplify to,

$$(A + (s_k + 2\lambda^2)I)\boldsymbol{w}_k = \boldsymbol{g}_k(\lambda), \quad \text{for} \quad k = 1, \ldots, n. \tag{36}$$

Finally, once we have solved for W, the reconstructed surface is recovered by the transformation,

$$Z = WU^{\mathrm{T}}. \tag{37}$$

The novelty of the expressions in Eq. (36) is twofold:

1. The equations involve only differential operators and diagonal matrices, meaning they are extremely sparse.

[1] Effectively we require only the Schur decomposition, which is a partial eigen-decomposition. In this case, because the matrix is symmetric, they are identical, and we refer to the eigen-decomposition due to its general familiarity.

2. The equations for each column of W are independent of the others, meaning that they can be computed in parallel. That is, a quad-core processor could solve for four of the columns of W simultaneously.

Since this is the only online portion of the algorithm, the computation time can be reduced to very reasonable times. The coefficient matrix of each linear system has the form,

$$A_k = A + (s_k + 2\lambda^2)I \tag{38}$$

$$= D_y^{\mathrm{T}} D_y + (s_k + 2\lambda^2)I \tag{39}$$

which has a sparsity ratio (when Z is $m \times n$) of

$$S(m) = \frac{3m+4}{m^2} \tag{40}$$

which is to say that when $m > 300$, less than 1% of the coefficient matrix is populated (non-zero). In this sense, for large surfaces, the efficiency of solving these equations is greatly improved.

3.2. Algorithm summary

While the derivation of the algorithm is somewhat involved, the computational algorithm itself as derived is relatively straightforward as evidenced by the following pseudo-code. It is divided into portions which can be computed off-line, and the remaining portion which is computed online for each given reconstruction task:

Off-line:

1. Form the differential operators D_x and D_y.
2. Compute the eigen/Schur-decomposition of the matrix $D_x^{\mathrm{T}} D_x$.

Online:

Given the measured gradient, $(\hat{Z}_x, \hat{Z}_y)$:

3. Form the matrix G.
4. For $k = 1, \ldots, n$ (Or in parallel), form the matrices A_k and solve the linear systems,

$$A_k \boldsymbol{w}_k = \boldsymbol{g}_k \tag{41}$$

5. Recover the reconstructed surface as $Z = WU^{\mathrm{T}}$.

The dominant portion of the algorithm is the Schur-decomposition in the offline portion, which is the $\mathcal{O}(n^3)$ portion of the computation.

4. Numerical testing

4.1. Computation time

To demonstrate the improvement in computation time, we have compared three approaches. The first, is solving the least squares problem by vectorization, which is the most common approach in the literature [16,18,19]. Since for an $m \times n$ surface this involves solving an $2mn \times mn$ linear system of equations, this method is inefficient, even using sparse methods. The second method is that which was recently proposed in [20], by solving the Sylvester equation in Eq. (23) by means of the Bartels–Stewart algorithm. Thirdly, we have also compared the integration based method of Section 2.2; while they are usually fast, they however do not provide very good results due to the fact that they are not least-squares approximations. Finally, these methods are compared to the total computation time of the new algorithm. This comparison is shown in Table 1.

Clearly, the vectorization method takes times on the order of minutes to compute the reconstruction. Methods as [18,16,19] are based on this principle, are consequently $\mathcal{O}(n^6)$ algorithms, and hence can be no more efficient than the times under "Vectorization" in Table 1. In fact, the methods [18,19] are iterative methods using vectorized reconstruction at each step, and cannot reconstruct surfaces with $n > 300$, even on a modern computer. The Sylvester equation based method is an $\mathcal{O}(n^3)$ method, and produces reasonable times, yet still leaves something to be desired. As for the integration based methods, they are reasonably fast. Clearly, since they surpass the new algorithm for about $n > 1000$, the complexity of the integration scheme is less than $\mathcal{O}(n^3)$. Finally, the new method, while also an $\mathcal{O}(n^3)$ method, produces results more than twice as fast than the conventional solution to the Sylvester equation for the larger surfaces. The true advantage of the algorithm lies in the fact that most of this computation, however, can be done off-line.

Table 1
Improvements in algorithm timing.

Surface size	Vectorized	Sylvester [20]	Integration	New
400×400	39.063 s	0.782 s	0.844 s	0.406 s
600×600	95.706 s	2.185 s	1.717 s	1.109 s
800×800	170.545 s	5.308 s	2.873 s	2.358 s
1000×1000	266.120 s	10.926 s	4.340 s	4.464 s
1200×1200	382.576 s	19.899 s	6.155 s	7.747 s
1400×1400	518.699 s	32.043 s	8.358 s	12.435 s

Table 2
Breakdown of the new algorithm's timing.

Surface size	Total time	Online time (Eq. (36))
400×400	0.406 s	0.094 s
600×600	1.109 s	0.188 s
800×800	2.358 s	0.298 s
1000×1000	4.464 s	0.453 s
1200×1200	7.747 s	0.594 s
1400×1400	12.435 s	0.829 s

To further demonstrate the power of the new algorithm, we have broken down the computation into its total time and the time required for the online portion in Table 2. Since the dominant portion of the algorithm is the eigen/Schur-decomposition, the majority of the computation is done off-line. The online portion is clearly only about one tenth of the total computation time. Furthermore, by introducing parallel computing into the online portion, the times in Table 2 can be reduced further still. If these values are compared to those in Table 1, we can see that the new algorithm improves on the state of the art by about two orders of magnitude, and previous methods based on vectorization are simply not comparable.

4.2. Least-squares properties

To rate the quality of reconstruction of the new method, we have tested various methods with respect to how they reconstruct an analytic surface, whose gradient is subject to synthetic Gaussian noise. The test surface is a sum of Gaussian "bells", and is shown in Fig. 3. This type of surface provides a good example, since it is non-polynomial (transcendental) and most numerical approximations of derivatives/integrals are polynomial based.

Since the surface and its gradient are known exactly, we may directly compare reconstructions to the true surface by computing the reconstruction residuals as,

$$R_{\mathrm{rec}} = Z_{\mathrm{rec}} - Z_{\mathrm{true}}. \tag{42}$$

Fig. 4 shows the residuals of four different methods; the integration based method discussed here, the method of Simchony et al. [15], the method of Frankot and Chellappa [9], and the newly

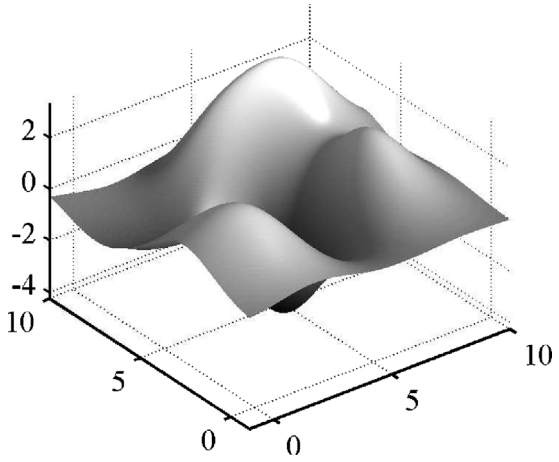

Fig. 3. The test surface for least squares reconstruction from gradient fields. Its gradient has an analytic form, and is thus known exactly.

proposed method. The integration method provides relatively poor results, since it only provides a least squares approximation in one direction (in this case the x-direction). The Simchony and Frankot–Chellappa methods provide least squares approximations, however both suffer from systematic defects. The method of Simchony et al. uses forward differences, and is hence only first order accurate. The method of Frankot and Chellappa assumes the reconstructed surface has periodic boundary conditions. Finally, the new method provides a residual which is expected of a least squares method: a residual which itself is purely stochastic. To demonstrate this, the histograms of the residuals are shown in Fig. 5. The histograms of errors of the integration method and the Frankot–Chellappa method show large errors, with a largely irregular distribution. The Simchony et al. method shows smaller errors however, still with a systematic skewness. Finally, the new method is the only method which results in a symmetric Gaussian distribution of residual errors, which is to be expected of a least squares approximation.

4.3. Photometric stereo reconstruction results

There are some examples of data sets in the literature, which are used to test surface reconstruction from gradients for the task of Photometric Stereo. For example, the "Mozart" data set, which is

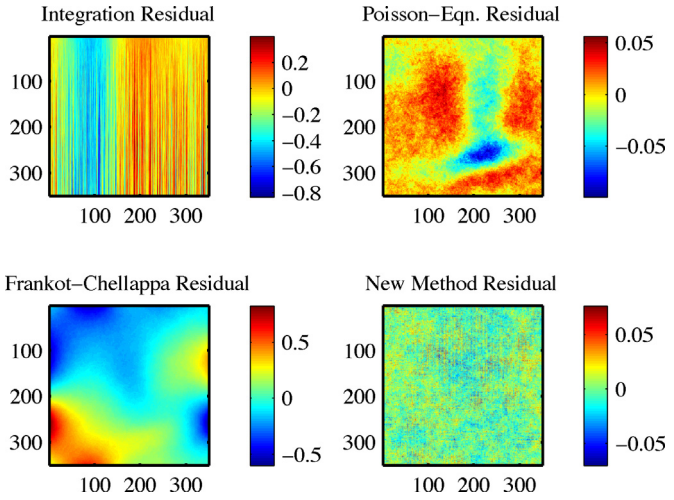

Fig. 4. The reconstruction residuals w.r.t. to the test surface in Fig. 3. All methods show systematic deviations in their residuals, whereby only the new method provides a purely stochastic residual. Note the different scales of the errors in the various reconstructions.

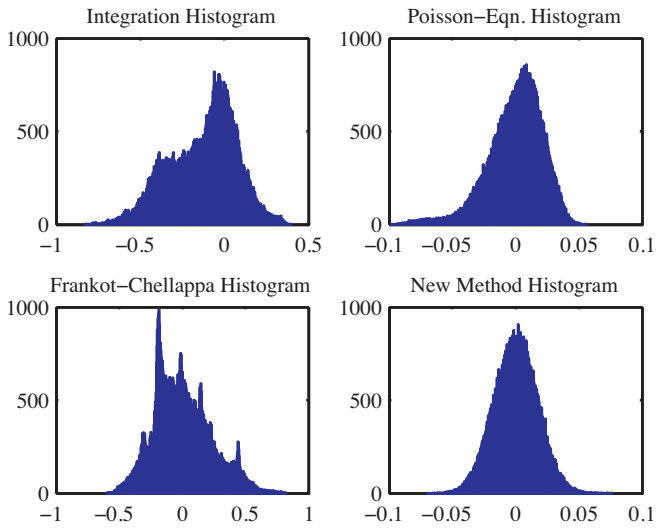

Fig. 5. Histograms of the reconstruction residuals in Fig. 4. Only the new method yields residuals with a Gaussian distribution. Note the different scales of the errors in the various reconstructions.

used as a basic example of Photometric Stereo; see Fig. 6. This is a straightforward example, since the bust is approximately Lambertian, and therefore satisfies the basic assumptions of Photometric Stereo. Results are shown of the global least squares solution as well as the Tikhonov regularized solution. Using $Z_0 = 0$ tends to flatten the surface, the effects of which are demonstrated.

If, however, one wishes to apply Photometric Stereo in an industrial environment, we must work with much more difficult examples. Working with the apparatus shown in Fig. 1, we have obtained the necessary images to compute the gradient of a test surface; the test surface is metallic, with many different textures, such as rust. Further, due to physical limitations, the lighting is not completely uniform over the surface. The measured gradient field is shown in Fig. 7.

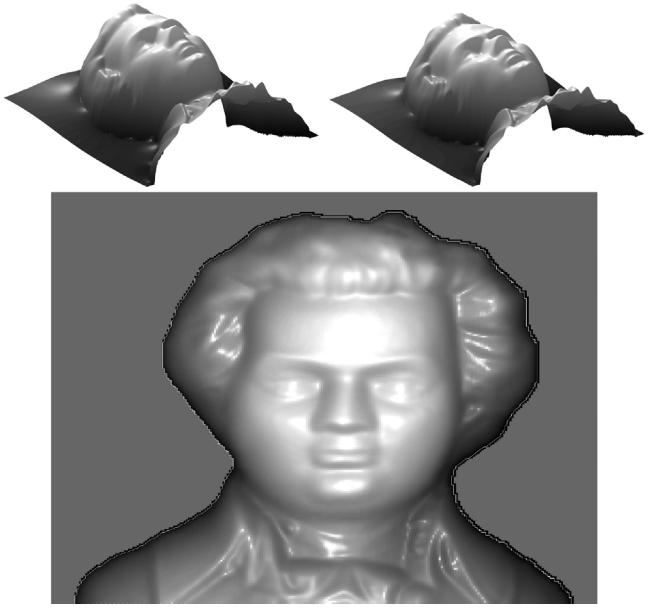

Fig. 6. The reconstruction of the standard test data set "Mozart" with the new algorithm. Top-left is the global least squares reconstruction. Top-right is the Tikhonov regularized solution, which tends to be flattened when the a priori estimate is assumed to be zero. Bottom is the front view of the Tikhonov reconstruction, which better shows the reconstructed details. These results are a substantial improvement as compared to published results of other less-efficient algorithms presented, for example, in [18,19].

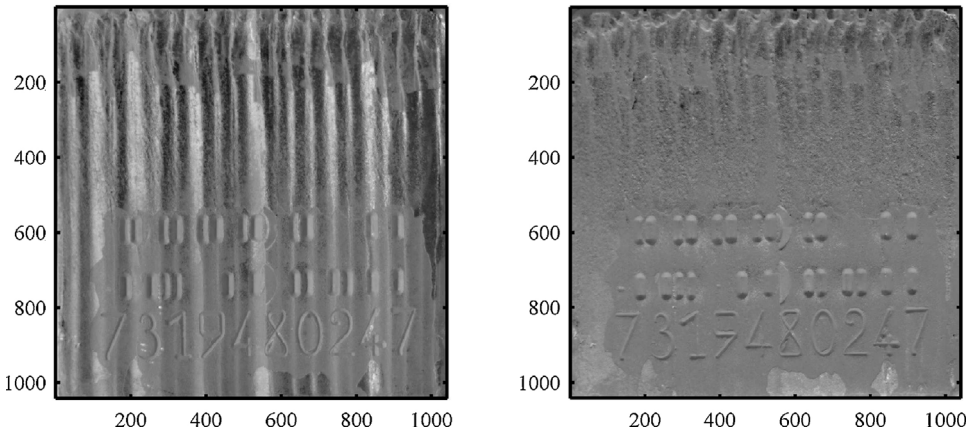

Fig. 7. The measured gradient field $(\hat{Z}_x, \hat{Z}_y)$ using an Industrial Photometric Stereo setup.

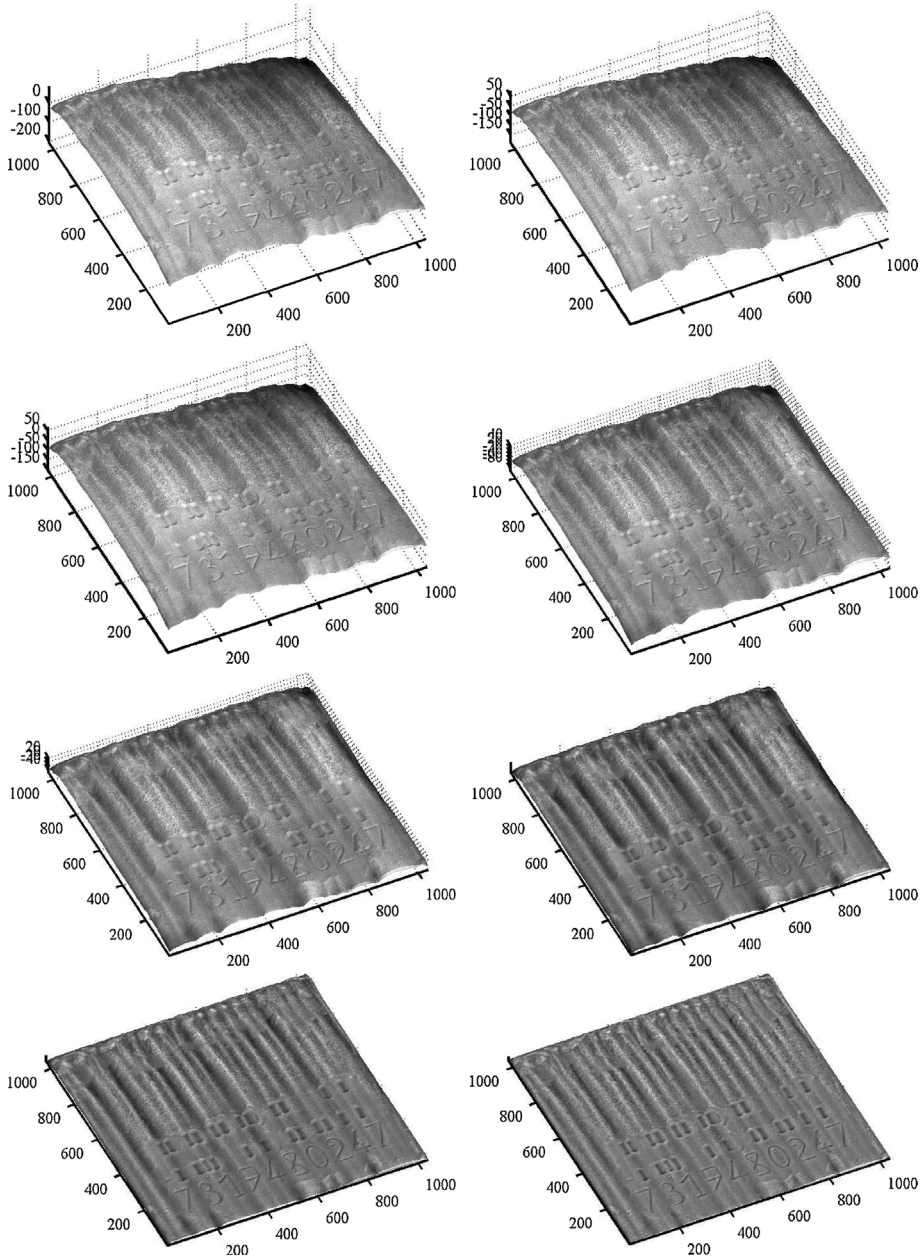

Fig. 8. Reconstruction from images of size 1040×1040. Top to bottom, left to right, solutions with Tikhonov regularization with $\lambda = 0.0001, 0.001, 0.002, 0.005, 0.01, 0.02, 0.05, 0.1$. An image of the corresponding real surface is shown in Fig. 2.

In an effort to reconstruct as much detail as possible, an industrial camera with a resolution of 1040×1040 was used. Clearly, the surface of a steel bar is not Lambertian, and images under even controlled conditions can have specular reflections. The results of the reconstruction are shown in Fig. 8. In this example, it is known that the steel plate is relatively flat, and thus Tikhonov regularization can be used to greatly improve the reconstruction. Results are shown for values of the regularization parameter of $\lambda = 0.0001, 0.001, 0.002, 0.005, 0.01, 0.02, 0.05, 0.1$, i.e., varying quite largely in magnitude. However, generally as is the case with Tikhonov regularization, the larger the value of λ, the flatter the reconstructed surface (i.e., the smaller the deviation from $Z_0 = 0$). The first reconstruction (very small λ) is essentially the global least squares solution, which shows a systematic deviation from the true surface. However, the solution with the largest λ has flattened out the surface, but not the details. Note that the ridges on the surface are in fact part of the true geometry of the surface (cf. Fig. 2). Thus, Tikhonov regularization can be used to suppress the low frequency, systematic errors in the reconstruction problem. In this case, the portion we are interested in – the human readable code – is more visible than in any of the other reconstructions.

5. Conclusions

In this paper, we have proposed a new approach to computing the Tikhonov regularized solution to reconstructing a surface from its measured gradient field. In terms of online computation, the new algorithm allows for the reconstruction of mega-pixel sized surfaces in under 1 s. These results improve on the state-of-the-art by orders of magnitude. It is the first algorithm which is viable for regularized reconstruction in Industrial Photometric Stereo.

Acknowledgement

The authors would like to thank Georg Jaindl for acquiring the Photometric Stereo images [24], as well as the setup photos and figures.

References

[1] R. Woodham, Photometric method for determining surface orientation from multiple images, Optical Engineering 19 (1) (1980) 139–144.
[2] N. Alldrin, T. Zickler, D. Kriegman, Photometric stereo with non-parametric and spatially-varying reflectance, in: Computer Vision and Pattern Recognition, IEEE, Anchorage, USA, 2008, pp. 1–8.
[3] T. Kuparinen, V. Kyrki, Optimal reconstruction of approximate planar surfaces using photometric stereo, Pattern Analysis and Machine Intelligence 31 (12) (2009) 2282–2289.
[4] H. Engl, M. Hanke, A. Neubauer, Regularization of Inverse Problems, Kluwer Academic Publishers, Dordrecht, NL, 2000.
[5] Z. Wu, L. Li, A line integration based method for depth recovery from surface normals, in: IEEE ICPR, IEEE, Rome, 1988, pp. 591–595.
[6] R. Klette, K. Schlüns, A. Koschan, Computer Vision: Three-Dimensional Data from Images, Springer, Singapore, 1998.
[7] A. Robles-Kelly, E. Hancock, A graph-spectral method for surface height recovery, Pattern Recognition 38 (2005) 1167–1186.
[8] M. Smith, Surface Inspection Techniques, Engineering Research Series, Professional Engineering Publishing Ltd., Suffolk, 2001.
[9] R. Frankot, R. Chellappa, A method for enforcing integrability in shape from shading algorithms, IEEE PAMI 10 (4) (1988) 439–451.
[10] P. Kovesi, Shapelets correlated with surface normals produce surfaces, in: IEEE ICCV, Beijing, (2005), pp. 994–1001.
[11] B. Karaçalı, W. Snyder, Reconstructing discontinuous surfaces from a given gradient field using partial integrability, Computer Vision and Image Understanding 92 (2003) 78–111.
[12] B. Horn, M. Brooks, The variational approach to shape from shading, Computer Vision, Graphics, and Image Processing 33 (1986) 174–208.
[13] F. Dorr, The direct solution of the discrete Poisson equation on a rectangle, SIAM Review 12 (2) (1970) 248–263.
[14] J.-D. Durou, F. Courteille, Integration of a normal field without boundary condition, in: Proc. 1st Workshop on PACV, Rio de Janeiro, Brazil, 2007.
[15] T. Simchony, R. Chellappa, M. Shao, Direct analytical methods for solving Poisson equations in computer vision, IEEE PAMI 12 (5) (1990) 435–446.
[16] I. Horovitz, N. Kiryati, Depth from gradient fields and control points: bias correction in photometric stereo, Image and Vision Computing 22 (2004) 681–694.
[17] M. Harker, P. O'Leary, Least squares surface reconstruction from measured gradient fields, in: CVPR 2008, IEEE, Anchorage, AK, 2008, pp. 1–7.
[18] H.-S. Ng, T.-P. Wu, C.-K. Tang, Surface-from-gradients without discrete integrability enforcement: a Gaussian kernel approach, IEEE PAMI (2013) (in press).
[19] A. Agrawal, R. Raskar, R. Chellappa, What is the range of surface reconstruction from a gradient field? in: ECCV 2006, LNCS, Graz, Austria, 2006, pp. 578–591.
[20] M. Harker, P. O'Leary, Least squares surface reconstruction from gradients: direct algebraic methods with spectral, Tikhonov, and constrained regularization, in: IEEE CVPR, IEEE, Colorado Springs, CO, 2011, pp. 2529–2536.
[21] R. Adams, Calculus: Several Variables, sixth ed., Pearson Addison Wesley, 2006.
[22] R. Burden, J. Faires, Numerical Analysis, eighth ed., Thomson Learning, Inc., 2005.
[23] P. Hansen, D. O'Leary, The use of the L-curve in the regularization of discrete ill-posed problems, SIAM Journal on Scientific Computing 14 (6) (1993) 1487–1503.
[24] G. Jaindl, Development of a photometric stereo measurement system, University of Leoben, 2009 (Diploma thesis).